Atmospheric Environment 43 (2009) 2700–2708

Contents lists available at ScienceDirect

Atmospheric Environment

journal homepage: www.elsevier.com/locate/atmosenv

Columnar optical properties of tropospheric aerosol by combined lidar and sunphotometer measurements at Taipei, Taiwan

Wei-Nai Chen [a,*], Yi-Wei Chen [b], Charles C.K. Chou [a], Shih-Yang Chang [c], Po-Hsiung Lin [b], Jen-Ping Chen [b]

[a] Research Center for Environmental Changes, Academia Sinica, Taipei, Taiwan
[b] Atmospheric Science Department, National Taiwan University, Taipei, Taiwan
[c] Department of Public Health, Chung Shan Medical University, Taichung, Taiwan

ARTICLE INFO

Article history:
Received 9 December 2008
Received in revised form
19 February 2009
Accepted 26 February 2009

Keywords:
Lidar
Sunphotometer
Aerosol
Lidar ratio
Angstrom exponent
Depolarization

ABSTRACT

Vertical extinction profiles and columnar optical properties (optical depth, Angstrom exponent, lidar ratio, and particle depolarization) of aerosols were obtained by simultaneous measurements with a depolarization lidar and a sunphotometer at Taipei, Taiwan from February 2004 to January 2006. Columnar optical depths are high in Feb–Apr (0.61–0.75) by sunphotometer measurements. Lidar measurements show the contribution of aerosols in the free atmosphere on columnar optical depths are about 44–50% in Feb–Apr and about 26–37% in other months. Back-trajectory analyses and depolarization measurements show almost all of non-spherical aerosols originated from Northwest China which indicate Asian dusts frequently transported to Taipei from dust source regions in the free atmosphere. Aerosols with depolarization lower than 5% are found mostly originated from South China or Southeast Asia. Good correlations between columnar lidar ratio, particle depolarization, and Angstrom exponent are found for cases that columnar water vapor less than 1.5 cm. The effect of water vapor on particle depolarization is briefly discussed.

1. Introduction

East Asia is characterized by high and rapid growing anthropogenic emissions resulting from the high population and energy consumption in the region. These gaseous and aerosol components exert an essential influence upon the atmosphere modifying its structure, properties and components. Both natural and anthropogenic aerosols can affect climate directly by solar radiation scattering and absorption (Charlson et al., 1992) and indirectly by their abilities to nucleate cloud droplets (Twomey, 1991). In Taiwan, a major natural component of atmospheric aerosol is mineral dusts from arid and semi-arid regions of Mainland China (Liu and Shiu, 2001) and the major anthropogenic components are sulfate and biomass-burning smoke from local sources or Southeast Asia (Wang et al., 2007).

Aerosol optical depth is a main parameter of the aerosols that has significant impact on the climate. Light scattering and absorption by aerosols cause reduction in solar radiation and influence visual air quality, thereby adversely impacting visibility and the quality of the atmosphere (Seinfeld and Pandis, 1998). Thus, the characterization of aerosol properties is crucial to understand their influence on the Earth-atmosphere radiation budget. Furthermore, the microphysical characteristics of aerosols can be classified according to their geographical origin such as urban, rural, marine or continental, and also to local meteorological conditions (Müller et al., 2007). In this paper, we present the intensive (independent on concentration) columnar optical properties of aerosols such as optical depths, Angstrom exponents, extinction-to-backscatter ratios (so called lidar ratio), and particle depolarizations over Taipei determined by lidar and sunphotometer. Lidar ratio is usually treated as one of characteristics of particle (Müller et al., 2007) which ranges from 20 to 80 for urban aerosols, 45–65 sr for biomass burnings, and 30–40 sr for Asian dusts (Ansmann et al., 1992; Takamura et al., 1994; Anderson et al., 2000; Liu et al., 2002). Angstrom exponent is a good indicator of the size of particles (Schuster et al., 2006). Higher values (greater than 2) are typically observed for accumulation mode particles and lower values (near 0) have been observed for coarse mode particles such as dusts (Wang et al., 2004). The depolarization was widely considered as indicator of the non-sphericity of particles such cirrus and dusts (Sassen, 1991; Iwasaka et al., 2003).

In Taiwan, distinct correlations between columnar optical depths and concentration of aerosols observed in Taipei and Tainan had been noticed might be owing to non-vertically well-mixed tropospheric aerosols (Shiu et al., 2006). Therefore, to obtain aerosol vertical profile is important in understanding the variation

* Corresponding author. Tel.: +886 226539885; fax: +886 227833584.
E-mail address: wnchen@rcec.sinica.edu.tw (W.-N. Chen).

1352-2310/$ – see front matter © 2009 Elsevier Ltd. All rights reserved.
doi:10.1016/j.atmosenv.2009.02.059

of ground pollutants. Lidar is a powerful technique for active remote sensing of the vertical profile of troposphere with high temporal and spatial resolution. However, retrieval of the aerosol extinction profile from backscattered lidar measurements requires knowledge of the aerosol lidar ratio (Klett, 1981; Fernald, 1984). Lidar ratio is a complicated function depends on the size distribution, shape and composition of the aerosols. In the absence of direct lidar ratio measurements, columnar lidar ratio may be obtained by constraining the vertical integral of lidar-derived aerosol extinction coefficients with independent aerosol optical depth measurements (Welton et al., 2002; Chazette, 2003). In this study, this method was applied to lidar inversion with simultaneous columnar aerosol optical depth from sunphotometer.

In this study, columnar optical depths are large in Feb–Apr (0.61–0.75) by sunphotometer measurements. Lidar vertical extinction/depolarization profiles and back-trajectory analyses reveal the abundant of optical depths are mostly owing to anthropogenic aerosols or dusts in the free atmosphere transported from Southern China or Northwest China. The inter-relationships between the intensive optical properties are discussed. We found good correlations between columnar lidar ratio, particle depolarization; and Angstrom exponent are found for cases that columnar water vapor less than 1.5 cm which implies both lidar ratio and depolarization ratio are dependent on particle size under dryer condition.

2. Instruments and methodology

Columnar aerosol optical properties and vertical extinction profiles are measured by a sunphotometer and a depolarization lidar installed at the Taipei Aerosol and Radiation Observatory (TARO) located in the campus of the National Taiwan University (25.014°N, 121.53°E). A set of aerosol and radiation measurements including PM_{10}, $PM_{2.5}$ (particulates of 10 and 2.5 μm or less respectively), lidar, and sunphotometer are conducted at TARO by the Research Center for Environmental Changes (RCEC), Academia Sinica to investigate physico-chemical characteristics of urban aerosols, and their influences upon the air quality and solar radiation budget in Taipei. TARO is located near the center of Taipei Basin, and the data provide aerosol characteristics from a subtropical metropolitan city. The geophysical location of TARO is shown in Fig. 1.

2.1. CIMEL sunphotometer

The columnar aerosol optical depth (AOD) was retrieved from the radiance measured by the CIMEL Electronique CE318-1 automatic sun-tracking sunphotometer. The CIMEL sunphotometer measurements include the radiances in seven spectral channels (340, 380, 440, 500, 675, 870, and 1020 nm). Direct solar radiation at 15-min intervals and sky radiation at 1-h intervals are recorded. As part of the AERONET project, data measured by the CIMEL are sent to U.S. NASA Goddard Space Flight Center for the retrievals of aerosol optical depth, water vapor, single-scattering albedo, asymmetry factor, and size distribution. CIMEL is calibrated during the summer, and the measurements are conducted only in October–May. AERONET data are available at three levels: level 1.0 (unscreened), level 1.5 (cloud screened) and level 2.0 (quality assured). In this study, the level 2.0 AOD, columnar Angstrom exponent (cÅ), and columnar water vapor (cW) are used for the present analysis. Columnar water vapor is precipitable water expressed in units of volume of liquid water per unit area ($cm^3\ cm^{-2}$). The precipitable water is about 5 cm near the equator and less than one tenth at the poles.

2.2. RCEC/ASNTU lidar

RCEC/ASNTU lidar is a depolarization lidar system employs the second and third harmonics of Nd:YAG laser at 532 nm and 355 nm co-funded by Research Center for Environmental Changes, Academia Sinica (hereafter RCEC) and Dept. of Atmospheric Science, National Taiwan University, Taiwan (hereafter ASNTU). The

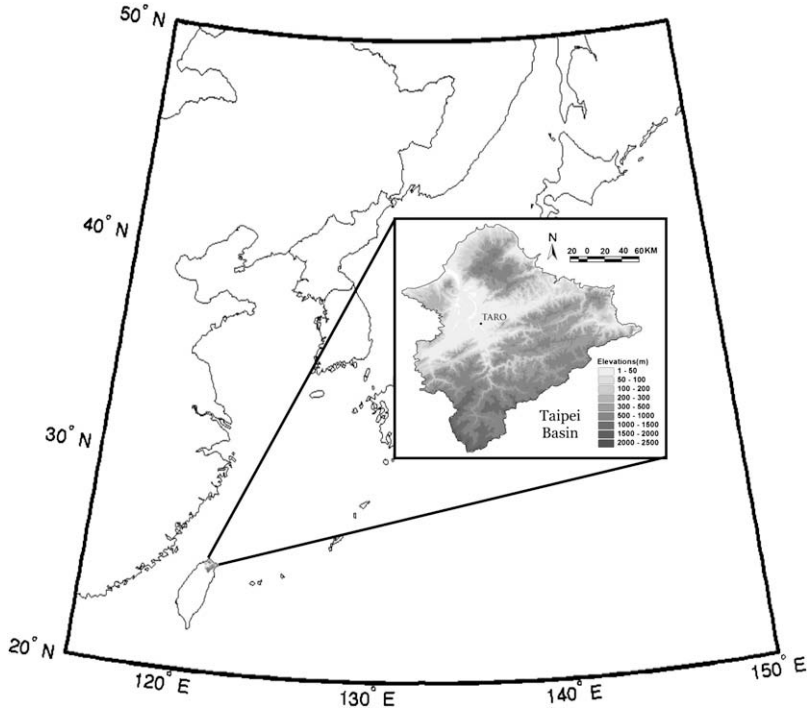

Fig. 1. Geographical location of TARO in Taipei Basin.

lidar system measures the vertical distribution of aerosol backscattering, extinction, and depolarization (at 532 nm) by detecting the Rayleigh/Mie backscattering of atmospheric molecules and aerosol particles. Detailed specification of this lidar is given in Table 1. During the study period, lidar measurements were carried out routinely under thick-cloud free condition. Lidar signals were acquired for every minute and were averaged for every 15 min to improve the signal to noise ratio.

The backscattering signal for elastic Rayleigh/Mie lidar is described by the lidar equation as follows:

$$P_R(\lambda,z) = P_L(\lambda)\frac{A}{z^2}[\beta_m(\lambda,z) + \beta_a(\lambda,z)] \times \exp\left[-2\int_{z_0}^{z}(\sigma_m(\lambda,z')+\sigma_a(\lambda,z'))\mathrm{d}z'\right] \quad (1)$$

where P_L is the power of laser; $P_R(z)$ is the number of photons received from altitude z; A is the system calibration factor (includes area of telescope and efficiencies of detector); β_m and β_a are the volume backscattering coefficients and σ_m and σ_a are the volume extinction coefficients of air molecular (m) and aerosol (a).

In this study, lidar equation is solved by Klett's inversion method expressed by following equations (Klett, 1981, 1985):

$$\beta(\lambda,z) = \frac{X(\lambda,z)}{\frac{X(\lambda,z_1)}{\beta(\lambda,z_1)} - 2\int_{z_1}^{z} S_a(\lambda)X(\lambda,z')\mathrm{d}z'} \quad (2)$$

$$X(\lambda,z) = P_R(\lambda,z)z^2\exp\left[-\int_{z_1}^{z}2(S_a(\lambda)-S_m)\beta_m(\lambda,z')\mathrm{d}z'\right] \quad (3)$$

where $\beta(\lambda, z) = \beta_a(\lambda, z) + \beta_m(\lambda, z)$; $\beta_a(\lambda, z_1)$ is the initial value of aerosol backscattering coefficient at height z_1; $S_a(\lambda)$ and S_m are lidar ratios (extinction-to-backscattering ratio) for aerosol and air molecular defined as $S = \sigma/\beta$. For air molecular, $S_m = 8\pi/3$. In this paper, z_1 usually ranges from 7 to 9 km, where is assumed to be aerosol free region (β_a close to 0). $S_a(\lambda)$ is abbreviated as S_λ for symbol simplification.

To overcome the uncertainty owing to unknown lidar ratio S_λ, aerosol optical depths measured by sunphotometer are applied as constraint for lidar signal inversion to derive columnar lidar ratio by substituting various S_λ into Eqs. (2) and (3) until column integrated aerosol extinction coefficients equal to AOD measurements. AODs for wavelength 355 nm and 532 nm are interpreted from AOD of 340–380 nm and 500–675 nm, respectively. The column integrated aerosol backscattering coefficient cB_λ can be simply obtained from the ratio of AOD to lidar ratio:

$$cB_\lambda = \int \beta_a(\lambda,z)\mathrm{d}z = AOD_\lambda/S_\lambda \quad (4)$$

And the column backscattering ratio cR_λ can be obtained accordingly:

$$cR_\lambda = 1 + \frac{cB_\lambda}{\int \beta_m(\lambda,z)\mathrm{d}z} \quad (5)$$

Two cases measured at 2004/2/18 10:09 LT (local time) and 2004/11/10 11:53 LT are shown in Fig. 2 to demonstrate aerosol vertical extinction profiles and column lidar ratios retrieved by method as mentioned above. Where aerosol columnar optical depths, columnar lidar ratios, and columnar particle depolarizations for cases observed on 2004/2/18 10:09 LT and 2004/11/10 11:53 LT are 0.86, 57 sr, 6.1% and 0.23, 42 sr, 5.3%, respectively. Follow the over lapping calibration method proposed by Wandinger and Ansmann (2002), our lidar signal is found being unreliable between 0 and 400 m owing to signal reducing problem caused by overlap between laser beam and field of view of telescope, lidar signal is unreliable between 0 and 400 m. Since aerosols are generally accepted to be well mixed inside mixing layer, therefore, only cases that mixing height higher than 400 m are selected and we assumed aerosols are well mixed below 400 m.

Depolarization ratio is an indicator of irregularly shaped particle. Lidar measurements reveal particles such as Asian dust, biomass burning, and sea-salt would exhibit clear depolarization properties owing to irregular shape. Depolarization is close to zero for spherical particle. For dry or crystallized sulfate, depolarization ratio is about 2% (Cooper et al., 1974; Sassen et al., 1989). Total depolarization ratio TDP is defined as ratio of perpendicular to parallel return signal (Sugimoto et al., 2002). In this study, column integrated lidar signals are applied to calculate columnar total depolarization ratio cTDP. To remove signal contributed by air molecules, columnar aerosol particle depolarization (cPD) was derived from the columnar total depolarization ratio cTDP and the columnar backscattering ratio cR_λ from the following equation (Liu et al., 2002):

$$cPD = \frac{cR_a \times \delta - \delta_m}{cR_a - 1} \quad (6)$$

where $\delta = cTDP/(1 + cTDP)$ and the molecular depolarization ratio δ_m is given as 1.4% (Weber et al., 1967; Young, 1980).

Table 1
Specifications of lidar.

Transmitter	
Laser	Nd:YAG (BigSky CFR400)
Wavelength	532/355 nm
Pulse energy	60 (maximum) mJ
Repetition rate	20 Hz
Receiver	
Telescope type	Cassegrain
Diameter	40 cm
Focal length	160 cm
Detector	PMT
Signal detection	Analog
Height resolution	7.5 m
Measured channel	
Rayleigh/Mie scattering	355 and 532 nm
Depolarization	532 nm

3. Results and discussions

Taipei is a subtropical city and usually is cloudy at winter and spring. During the experimental period, level 2.0 AOD is available in 155 days and we found 108 coincident lidar and sunphotometer measurements. Although few sunphotometer measurements are available in summer (June–September), there is no coincident lidar measurement.

3.1. Annual variation of columnar optical properties

The monthly mean columnar AOD (500 nm) for lidar and sunphotometer coincident measurements is shown in Fig. 3; each error bar indicates the standard deviation. In Fig. 3, it could be noticed that columnar AOD in Feb–Apr (0.61–0.75) is about two times higher than those in Oct–Jan (0.25–0.39). Higher monthly mean Angstrom exponents also found in Feb–Apr (1.40–1.49) which indicate aerosols were predominated by fine mode particles. Since

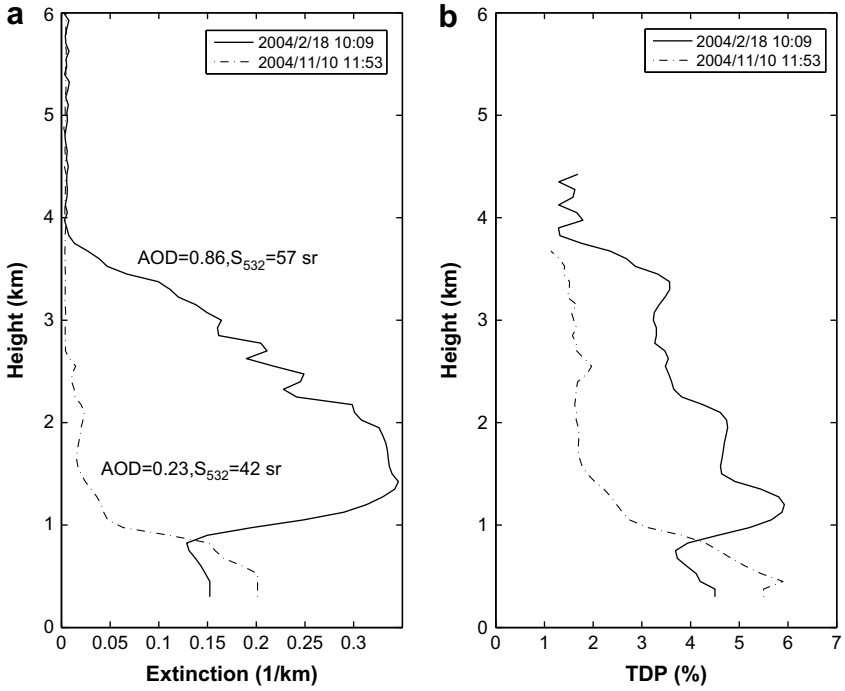

Fig. 2. Aerosol (a) extinction and (b) total depolarization ratio profiles measured at 2004/2/18 10:09 LT (local time, solid line) and 2004/11/10 11:53 LT (dashed line). Columnar aerosol optical depths, columnar lidar ratios, and columnar particle depolarizations for cases observed on 2004/2/18 10:09 LT and 2004/11/10 11:53 LT are 0.86, 57 sr, 6.1% and 0.23, 42 sr, 5.3%, respectively.

columnar AOD is directly related to aerosol physical characteristics such as number density or mass concentration, aerosol refractive index, and particle size (van de Hulst, 1957). In order to investigate the AOD in Feb–Apr, coincident surface ground aerosol mass concentrations PM_{10} and $PM_{2.5}$ measured at TARO, columnar Angstrom exponent and water vapor from sunphotometer are listed in Table 2 as references. Where columnar Angstrom exponent and water vapor are used to infer information about particle size and relative humidity.

The high values of AOD are found not related to columnar water vapor. Aerosols would grow up under higher relative humidity which would result higher scattering cross-section. In Table 2, it could be noticed that water vapor is lower in Dec–Apr (1.8–2.8 cm) and higher in May, Oct, and Nov (3.6–4.0 cm). Meanwhile, Angstrom exponent is found higher in Feb–Apr (1.40–1.49) and lower (1.22–1.32) in other months. Lower columnar water vapor found in Dec–Apr may be owing to winter monsoons, which bring dry and cold continental air from inner Asia. Higher columnar water vapor may be owing to Asian southwest monsoons, which bring moist air from Southeast Asia. Lower columnar water vapor and higher Angstrom exponents in Feb–Apr implies atmospheric columns are relative dryer and aerosols are relative smaller, therefore, this result suggests the high columnar AOD is not related to particle size owing to changes of columnar water vapor or relative humidity.

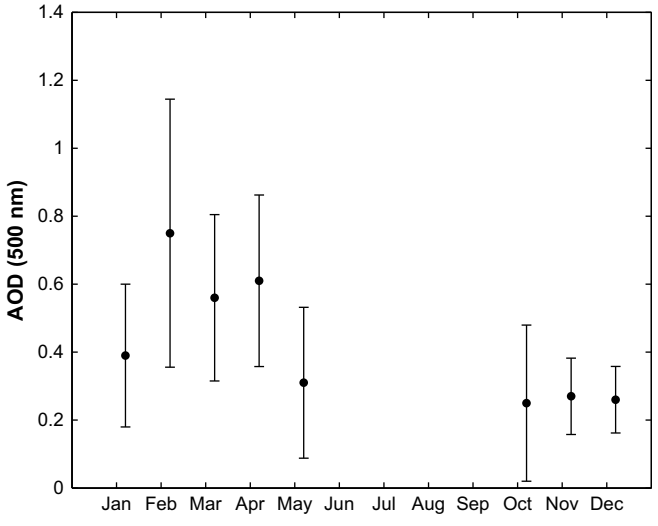

Fig. 3. Annual variation of columnar aerosol optical depth (AOD) for lidar and sunphotometer coincident measurements. Error bar indicates the standard deviation.

High columnar AOD in Feb–Apr may associate with pollutants long-range transporting along with northeasterly winter monsoon (Lin et al., 2004). Along with economic growth, East Asia has been a region of rapidly increasing emissions of air pollutants in the past decades. In the winter and spring, Taiwan and vicinity is often under the influence of northeasterly winter monsoon winds originating in Central Asia. The contribution of long-range transport pollutants originating from Mainland China to PM_{10} abundance in Northern Taiwan may range from 50% to 70% during the northeasterly monsoon (Lin et al., 2004). In Table 2, monthly mean PM_{10} and $PM_{2.5}$ in Jan–May in general are higher (up to 83 μg m^{-3} and 51 μg m^{-3}, respectively, except in February) than those in Oct–Dec (up to 63 μg m^{-3} and 33 μg m^{-3}, respectively) implies high PM_{10} and $PM_{2.5}$ is possibly owing to long-range pollutants transported from Mainland China. However, PM_{10} and $PM_{2.5}$ are not well correlated with columnar AOD (R^2 are 0.3 and 0.0, respectively) which indicate the increase of surface ground aerosol mass concentration is not enough to explain the high values of columnar AOD. The low correlations between columnar AOD and surface ground PM_{10} and $PM_{2.5}$ might be owing to increase of aerosols in the free atmosphere or solar activity because aerosols were elevated from surface ground to boundary layer by increase of

Table 2
Monthly mean values and standard deviations of CIMEL AOD (converted from 500 nm to 532 nm), columnar water vapors, column Angstrom exponents, surface aerosol mass concentrations (PM_{10} and $PM_{2.5}$), column lidar ratios S_{532} and S_{355}, column total depolarization ratio, column particle depolarization (cPD), $AOD_{1.2}$ (column integrated AOD for aerosol above 1.2 km), and ratios of $AOD_{1.2}$ to AOD.

Month	# of data	AOD (532 nm)	PM_{10} (μg m^{-3})	$PM_{2.5}$ (μg m^{-3})	Water Vapor (cm)	Angstrom (440–870 nm)
Jan	15	0.39 ± 0.20	70 ± 27	49 ± 24	2.3 ± 0.6	1.32 ± 0.20
Feb	18	0.75 ± 0.47	83 ± 40	N/A	2.2 ± 0.2	1.40 ± 0.19
Mar	17	0.56 ± 0.22	60 ± 18	31 ± 13	2.3 ± 0.9	1.49 ± 0.18
Apr	18	0.61 ± 0.24	71 ± 23	36 ± 16	2.8 ± 0.9	1.42 ± 0.20
May	8	0.31 ± 0.20	79 ± 17	51[a]	4.0 ± 0.7	1.26 ± 0.22
Oct	10	0.25 ± 0.21	50 ± 20	22 ± 10	3.6 ± 0.7	1.22 ± 0.12
Nov	7	0.27 ± 0.10	62 ± 12	31 ± 19	3.6 ± 0.2	1.30 ± 0.07
Dec	14	0.26 ± 0.09	63 ± 32	33 ± 20	1.8 ± 0.6	1.26 ± 0.22
Month	S_{532} (sr) (532 nm)	S_{355} (sr) (355 nm)	cTDP (%)	cPD (%)	$AOD_{1.2}$	$\frac{AOD_{1.2}}{AOD}$(%)
Jan	44 ± 11	42 ± 12	3.6 ± 1.1	4.7 ± 1.5	0.10	26%
Feb	52 ± 14	48 ± 18	4.6 ± 2.6	6.5 ± 3.8	0.38	50%
Mar	45 ± 7	44 ± 17	4.0 ± 1.9	5.9 ± 3.4	0.25	46%
Apr	46 ± 11	41 ± 13	4.3 ± 2.1	6.4 ± 4.1	0.28	45%
May	36 ± 11	38 ± 16	4.5 ± 0.7	6.3 ± 3.8	0.14	44%
Oct	33 ± 4	31 ± 5	2.0 ± 0.8	3.2 ± 4.4	0.09	37%
Nov	45 ± 17	43 ± 22	3.2 ± 1.8	4.1 ± 2.8	0.07	29%
Dec	33 ± 20	30 ± 7	3.9 ± 2.4	4.5 ± 3.8	0.08	27%

[a] Only one measurement is available.

convective fluxes. Therefore, aerosol vertical profiles measured by lidar are applied to investigate (see Section 3.2).

The winter monsoon not only brings air pollutants but also transports Asian dust to Taiwan and even to the Northwestern Pacific area (Sassen, 2002). On the monthly basis, Liu and Shiu (2001) had indicated the major increases of PM_{10} (around 8–12%) at Northern Taiwan in March–May are clearly associated with the Asian dust storm events. For identified Asian dust events, the impacts of Asian dusts on PM_{10} were estimated around 60–80% (Lin et al., 2005). Although dust particles might be not the only possible source of non-spherical particles (Murayama et al., 1999), our previous study (Chen et al., 2007a) had shown all of high depolarization episodes (TDP > 3.5%) observed at Taipei were caused by dust particles. Therefore, aerosol depolarization is applied as indicator of Asian dust in this study. In Table 2, values of monthly columnar total depolarization ratios (cTDP) and columnar particle depolarization (cPD) are 4.0–4.6% and 5.9–6.5% in Feb–May and cTDP and cPD are 2.0–3.9% and 3.2–4.7% in Oct–Jan which imply Taipei was suffered by Asian dusts more frequently in Feb–May than in Oct–Jan.

3.2. Vertical lidar profiles

In our previous study (Chen et al., 2007b), we had frequently observed aerosol layers with higher total depolarization ratio (TDP > 5%) in the free atmosphere at Northern Taiwan during dust seasons. The mean value of optical depth for identified dust layers is 0.23 ± 0.17 for wavelength of 355 nm (about 0.15 for 532 nm) which is about one fourth of columnar AOD in Feb–Apr as shown in Table 2. The monthly averaged vertical extinction measurements by RCEC/ASNTU lidar are shown in Fig. 4 and the monthly mean columnar lidar ratios for 532 nm and 355 nm are listed in Table 2. The lidar extinction profiles and columnar lidar ratios are calculated by method described in previous section. In Fig. 4, aerosol

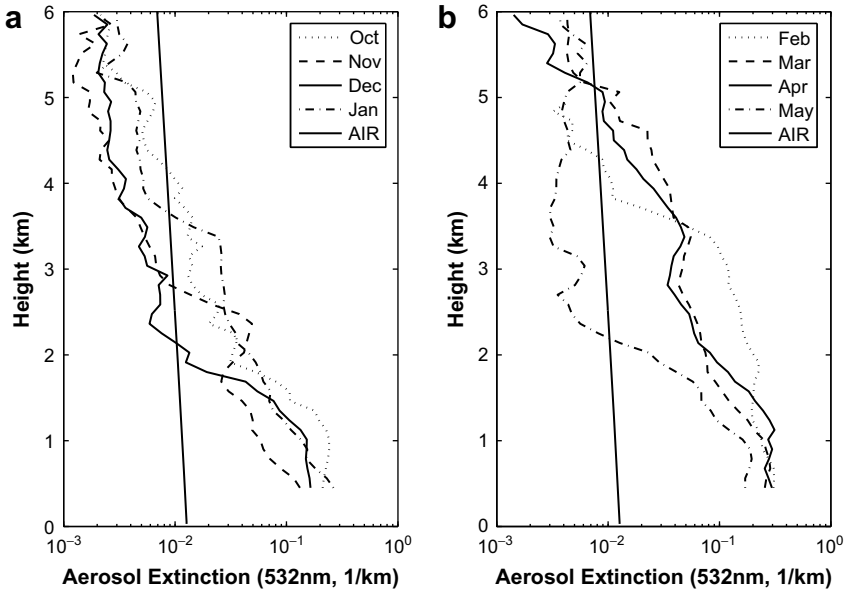

Fig. 4. Monthly mean vertical aerosol extinction profiles for (a) Oct–Jan and (b) Feb–May in logarithmic scale. Extinction profile of air molecular is also shown as reference.

extinction coefficients (at 532 nm) at altitude between 2 km and 3 km in Feb–Apr are about 0.05–0.1 km^{-1} which are apparently higher than extinctions in other months (up to 0.03 km^{-1}). In order to estimate the impact of aerosols in the free atmosphere on columnar AOD, aerosol extinction coefficients are integrated from 1.2 km to 6 km to represent aerosol optical depth in the free atmosphere, where 1.2 km is the maximum seasonal mean boundary layer height observed in autumn, winter, and spring (Chen et al., 2006). In this study, we also notice the uncertainty of boundary height for some cases might be larger than 200 m owing to existence of aerosols above boundary layer. Therefore, we used a fixed boundary height 1.2 km to estimate the impact of aerosols in the free atmosphere on columnar AOD. The monthly mean values of integrated aerosol extinction ($AOD_{1.2}$) and the fractions of $AOD_{1.2}$ to columnar AOD are listed in Table 2. The ratio of $AOD_{1.2}$ to columnar AOD is about 44–50% in Feb–May and 26–37% in Oct–Jan, which indicates about half of columnar AOD is contributed by aerosols in the free atmosphere in Feb–May.

The Hybrid Single Particle Lagrangian Integrated Trajectory Model (HYSPLIT) (Draxler and Rolph, 2003; Rolph, 2003) backward trajectory analysis was used to generate 3-day backward trajectories for air parcels arriving over Taipei at the altitude which we observed aerosol layers to track the air masses back to their source regions. Fig. 5 shows 72 h air mass back-trajectories for aerosols in the free atmosphere which extinction coefficients greater than 0.75 km^{-1}. Cases that TDP $\geq$ 5% and TDP $<$ 5% are represented as thick and thin lines, respectively. Fig. 5a shows 31 air mass back-trajectories for cases observed in Feb–May. Part of the air masses passed Asian dust source regions near Inner Mongolia, China. Lidar depolarization measurements also indicate TDP for all of those aerosol layers are greater than 5% which imply the existence of Asian dust particles. In Fig. 5a, most of air masses for TDP $\geq$ 5% descended from 6 to 8 km at latitude 105°E which imply dust layers were possibly lifted to high altitudes before transportation. These results consist with model simulation (Lin et al., 2007) which show the long-range transportation of Asian dust particles to the Taipei Basin usually is associated with dust storms, which lift particles up to high altitudes, and subsequently transport them over long distances by preventing the significant mixing, and the removal of particles from the surface.

Southeast Asia and South Asia are the highest biomass-burning regions. The peak emission season is spring for these two regions and for Southern China as well (Streets et al., 2003). Fig. 5a shows most of aerosol layers TDP $<$ 5% distributed at height between 1.5 and 4 km and their air masses passed Southern China or Southeast Asia. During their travel these air masses might cross biomass-burning regions and highly polluted regions in Southern China such as Pearl River Delta (PRD) (Hopkinson and Stern, 2002). Ma et al. (2003) reported purest biomass-burning plumes originated from Southeast Asia were measured at latitudes between approximately 15° and 25°N, and were found in layers at altitudes from 2 to 4 km asl during the Transport and Chemical Evolution Over the Pacific (TRACE-P) experiment. In the PRD region, Ansmann et al. (2005) had observed the top of the haze layer frequently reached to heights of 1.53 km by Raman lidar at Xinken (22.6°N, 113.6°W) on October 2004. Therefore, both anthropogenic pollutants and biomass-burning particles are possible source of aerosols that we observed in the free atmosphere. To distinguish biomass-burning aerosols from anthropogenic pollutants need more accurate measurement. By using multi-wavelength Raman lidar, Noh et al. (2008) had reported the smoke aerosols from Siberia, Russia can be separated from dust and anthropogenic pollution because of the spectral behavior of the lidar ratio (higher lidar ratio at 532 nm than at 355 nm) and the rather low Angstrom exponent values. However, aerosol optical properties such as depolarization and lidar ratio had not been well studied. Moreover, columnar aerosols are combinations of local anthropogenic aerosols and aerosols in the free atmosphere, therefore, it is difficult to identify aerosol type for aerosols in the free atmosphere transported from Southern China or Southeast Asia in this study.

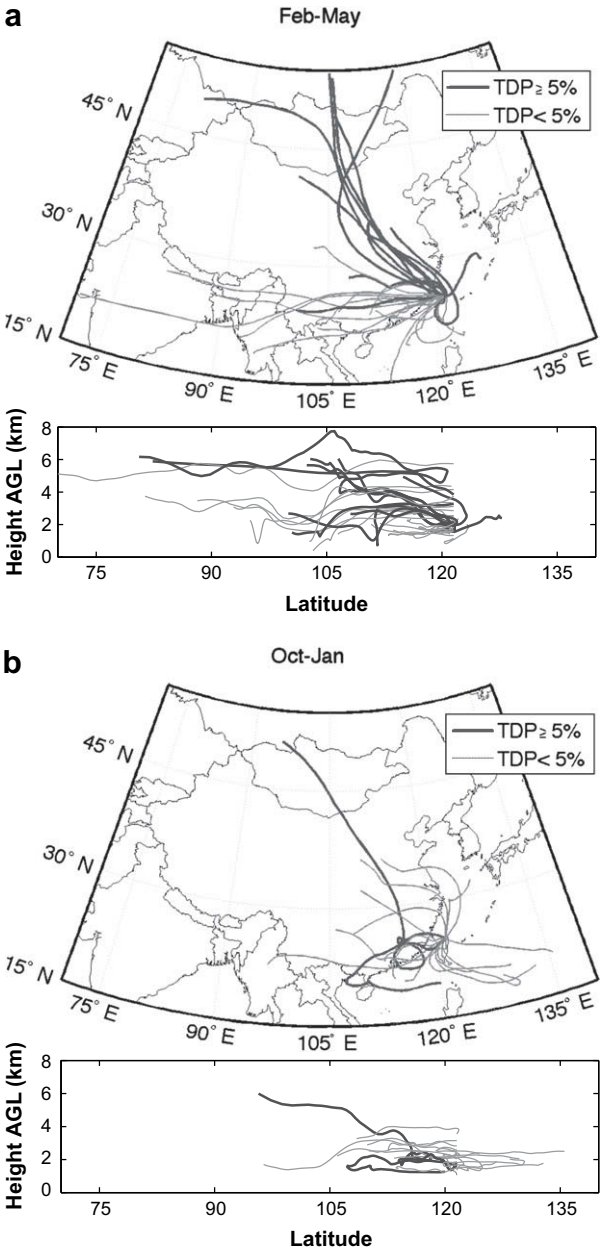

Fig. 5. 72 h HYSPLIT air mass back-trajectories for aerosol layers which maximum extinction greater than 0.1 km^{-1} observed in (a) Feb–May and (b) Oct–Jan. Cases that TDP $\geq$ 5% and TDP $<$ 5% are represented as thick and thin lines, respectively.

Seventeen air mass back-trajectories for aerosol layers observed in months Oct–Jan are shown in Fig. 5b. Most of air masses located at height between 2 and 4 km and mainly originated from Northwest China, Southern China, and Pacific Ocean. Total depolarization ratio for aerosols observed in these months in general are lower than 5% except two cases occurred on Dec. 12, 2004 and Jan. 4, 2006. Five days back-trajectories analyses for these two exceptions that identified for case occurred on Dec. 12, 2004 originated from dust source region in Northwest China; while for case occurred on Jan. 4, 2006 air mass came from Pacific Ocean via Southern China.

The aerosol sources for cases that air masses came from Pacific Ocean are not clear, more in situ measurements are needed to understand the possible sources. Nevertheless, since most of these air masses had passed Western Taiwan and Northern Philippine Sea, aerosols probably originated from Taiwan itself or Philippine.

3.3. Interrelationship between columnar optical properties and columnar water vapor

Lidar ratio is a complex light scattering property mainly determined by refractive index, particle size, and shape. Fig. 6 shows the distribution of all observed columnar lidar ratios at 532 nm and 355 nm, where S_{532} and S_{355} range from 19 to 92 sr and 12 to 90 sr. Monthly mean values of S_{532} and S_{355} are about 33–52 sr and 30–48 sr, respectively, which are close to lidar ratio at 532 nm measured at PRD and Beijing, China (47 ± 6 sr and 38 ± 7 sr, respectively) (Müller et al., 2007). In this study, we notice values of S_{355} are close to S_{532}. Good correlation $R = 0.82$ are found between S_{532} and S_{355} and the ratio of S_{355}/S_{532} is 0.94 (see Fig. 6). Similar correlation between lidar ratio at 355 nm and 532 nm had been observed for aerosols above PBL at Gwangju, Korea in autumn (Noh et al., 2008). Müller et al. (2007) also had reported the ratios of the lidar ratio at 355 nm and 532 nm for desert dusts, Arctic hazes, South/East Asian aerosols, and urban hazes at Central Europe are about 1–1.1; for urban hazes in North America is about 1.4 ± 0.2; and for forest fire smoke is 0.8 ± 0.2.

Lidar ratios of 30–60 sr are typically observed for anthropogenic and non-absorbing ammonium-sulfate particles (Franke et al., 2001). Ferrare et al. (2001) observed a high lidar ratio 68 ± 12 sr at 355 nm in the Southern Great Plains of North-central Oklahoma and reported that such a high ratio was associated with air masses from urban/industrial areas. To further investigate the physical implication of lidar ratio, Fig. 7a shows the scatter diagram of S_{532} versus columnar Angstrom exponent cÅ (440–870 nm) categorized by columnar particle depolarization cPD. The correlation between S_{532} and column Angstrom exponent cÅ for whole data set is $R = 0.48$, which indicates lidar ratio in general is weakly depended on particle size. In previous study (Chen et al., 2007b), we had noticed that lidar ratio of Asian dust is positively correlated with backscatter-related Angstrom exponent ($R = 0.69$). Therefore, in order to study the correlation between lidar ratio and Angstrom exponent, columnar particle depolarization cPD = 8% is selected as a threshold to classify identified dust events. Where cPD = 8% is the mean aerosol depolarization ratio for Asian dust episodes observed inside boundary layer at Taipei (Chen et al., 2007a). As shown in Fig. 7a, the correlation between cPD and cÅ for cases cPD ≥ 8% is $R = 0.73$. Ferrare et al. (2001) had reported a similar correlation ($R = 0.72$) between lidar ratio and Angstrom exponent for aerosols over the Southern Great Plains by using a Raman lidar and a sunphotometer. Takamura et al. (1994) had found higher lidar ratio when the contribution of fine mode aerosols is relatively large. Anderson et al. (2003) reported that values of lidar ratio at low RH were 50 ± 5 sr for fine mode dominated samples and 46 ± 8 sr for coarse mode dominated samples during the ACE-Asia IOP. Therefore, the positive correlation between lidar ratio and Angstrom exponent in identified dust events implies lidar ratio tends to decrease with decrease of effective particle size.

In Fig. 7a, it could be noticed that correlation between S_{532} and cÅ for non-evident dust cases (cPD < 8%) is low (about $R = 0.41$). Since particle depolarization of Asian dusts may be affected by water vapor (Sakai et al., 2002). Our previous study (Chen et al., 2007b) also shown dust particle depolarization tends to decrease under moist condition (RH > 70%). In this study, columnar water vapor (cW) retrieved from sunphotometer measurement was used to instead of relative humidity. The occurrence frequency

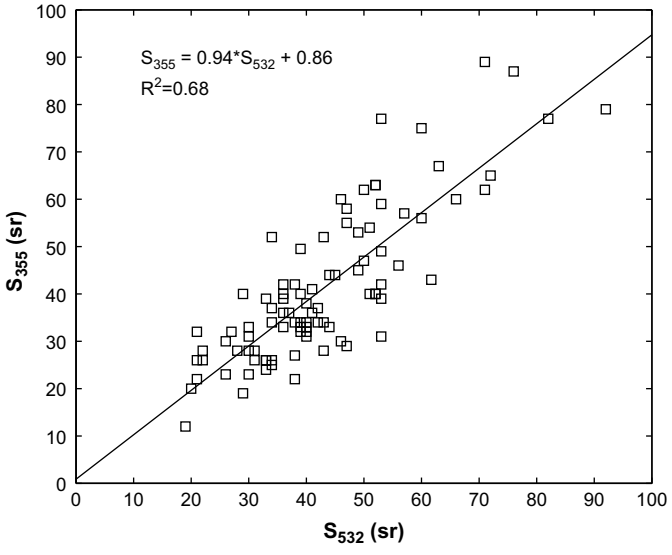

Fig. 6. Columnar lidar ratios at 532 nm and 355 nm. The correlation between S_{532} and S_{355} is $R = 0.82$.

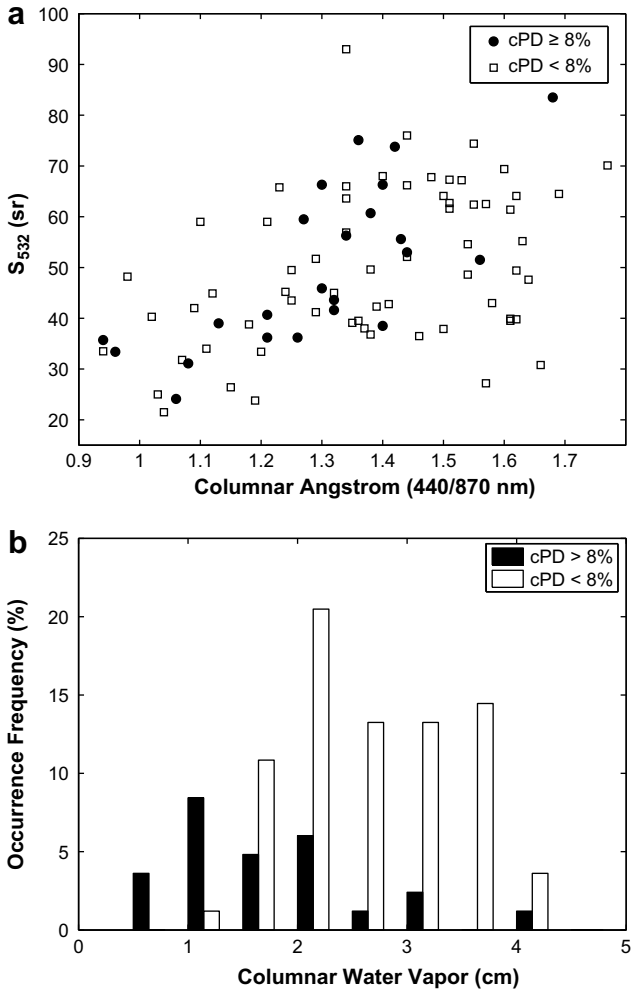

Fig. 7. (a) Scatter diagram of CIMEL Angstrom exponent (440–870 nm) and columnar lidar ratio for 532 nm categorized by columnar particle depolarization. Correlation coefficients between cÅ and S_{532} are $R = 0.73$ and 0.41 for cases cPD ≥ 8% and cPD < 8%. (b) Occurrence frequency histogram of observed columnar water vapors.

histograms of columnar water vapor for cPD greater or less than 8% are shown in Fig. 7b. Columnar water vapors for unidentified dust cases mainly distribute at moist region (cW ≈ 1.5–3.5 cm); while for evident dust cases apparently distribute at dryer region (cW ≈ 0.5–2 cm), which possibly because dusts are transported from the arid regions of China.

To further examine the influence of water vapor on optical properties, the scatter diagram of cPD versus cÅ and S_{532} categorized by columnar water vapor cW is shown in Fig. 8. For cases that cW less than 1.5 cm, the correlation coefficient for cPD versus cÅ is $R = -0.72$. Particle depolarization of dust is known to be dominated by its large size and irregular shape; this kind of negative correlations can be explained by the mixing of irregularly shaped coarse mode dusts and spherical-like fine mode particles (Sakai et al., 2002). cPD is also negatively correlated with S_{532} ($R = -0.74$) for cases cW < 1.5 cm. In other words, the intensive columnar optical properties such as cPD, cÅ, and columnar lidar ratio are correlated with each other under dryer condition (cW < 1.5 cm).

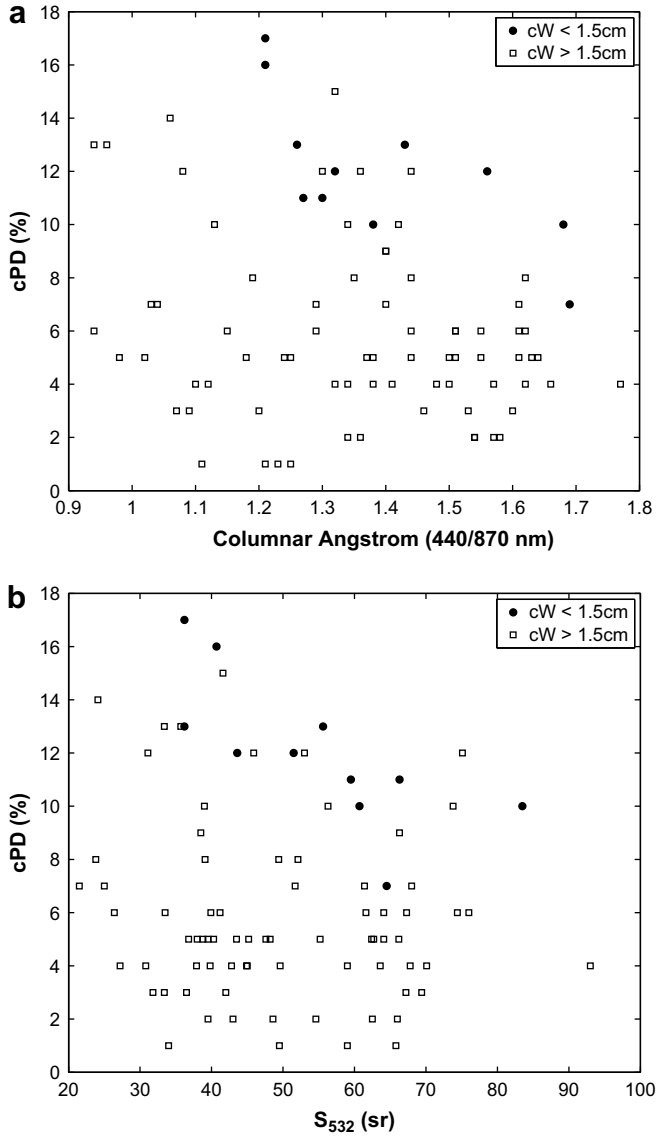

Fig. 8. Scatter diagram of columnar depolarization cPD versus (a) Angstrom exponent cÅ (440–870 nm) and (b) column lidar ratio S_{532}. The correlation coefficients for cPD versus cÅ and cPD versus S_{532} are $R = -0.72$ and -0.74, respectively for cW less than 1.5 cm.

No good correlation is found between cPD and cÅ, as well as cPD and S_{532} for cases cW greater than 1.5 cm ($R = -0.24$ and -0.15, respectively). This means that there is no correlation between intensive columnar optical properties when columnar water vapor is higher than 1.5 cm. This result may simply be caused by aerosols not well mixed inside the air column. However, aerosol hygroscopic properties might also be an important control factor. Numerical simulation (Ackermann, 1998) and Raman lidar measurement (Ferrare et al., 2001) had shown lidar ratio of continental aerosols tend to increase with increasing of relative humidity. In situ measurement (Anderson et al., 2000) found weak dependence between lidar ratio and relative humidity for urban aerosols. Therefore, scattered relationship between lidar ratio and Angstrom exponent might be possibly owing to relative humidity because both refractive index and particle size have changed. The effect of relative humidity on depolarization might be explained by external mixture of irregularly shaped dusts and spherical-like aerosols. Because of aerosol hygroscopic properties, the overall depolarization would be decreased owing to increase of scattering cross-section of spherical-like aerosols under moist environment. Another possibility for the scattered relationship between cPD and cÅ is the mineral particle turns to large spherical particle after coated with aqueous solution (Sakai et al., 2002), and then the depolarization decreases accordingly.

4. Conclusion remarks

Using simultaneous lidar and sunphotometer measurements, the columnar optical properties of aerosols such as optical depth, Angstrom exponent, lidar ratio, and particle depolarization observed in Taipei are studied. Columnar optical depth AOD in Feb–Apr is about 0.61–0.75 and in Oct–Jan is about 0.25–0.39. Comparing with surface ground aerosol concentrations (PM_{10} and $PM_{2.5}$) and lidar vertical extinction profiles, we found the high AOD in Feb–Apr is owing to increasing of aerosols in the free atmosphere. Lidar measurement shows the contribution of aerosols in the free atmosphere on columnar AOD is about 44–50% in Feb–Apr and is about 26–37% in other months. For cases observed in Feb–May, lidar depolarization measurements and HYSPLIT back-trajectory analyses show most of aerosols with total depolarization ratio TDP $\geq$ 5% mainly originated from dust regions in Northwest China. Whereas, aerosols with lower TDP < 5% are found mainly originated from Southern China or Southeast Asia, which imply that these aerosols are possibly biomass-burning smokes or anthropogenic aerosols.

Monthly mean values of columnar lidar ratio are about 33–52 sr and 30–48 sr for 532 nm and 355 nm, respectively. Inter-comparison between intensive columnar optical properties shows both columnar Angstrom exponent and columnar lidar ratio are well correlated with columnar particle depolarization for cases that columnar water vapor is less than 1.5 cm, which is similar to Asian dusts found in the free atmosphere. There is no good correlation between columnar particle depolarization, Angstrom exponent, and lidar ratio for cases with columnar water vapor greater than 1.5 cm. It is possibly owing to inhomogeneity of aerosol in air column, although water vapor might play important role because particle depolarization, Angstrom exponent, and lidar ratio would change under moist conditions. More in situ or laboratory experiments are needed to the effect of water vapor on aerosol properties.

Acknowledgments

This work was supported by the Nation Science Council of Taiwan, R.O.C. through grants NSC-90-2119-M-002-013, NSC-94-EPA-Z-008-003, NSC-94-2111-M-001-004, and NSC-95-2111-M-001-004. Partial funding support for the lidar instrument from the

College of Science, National Taiwan University is greatly appreciated. The authors gratefully acknowledge the NOAA Air Resources Laboratory (ARL) for the provision of the HYSPLIT transport and dispersion model and/or READY website (http://www.arl.noaa.gov/ready.html) used in this publication.

References

Ackermann, J., 1998. The extinction-to-backscatter ratio of tropospheric aerosol: a numerical study. Journal of Atmospheric and Oceanic Technology 15, 1043–1050.

Anderson, T.L., Masonis, S.J., Covert, D.S., Ahlquist, N.C., Howell, S.G., Clarke, A.D., McNaughton, C.S., Aug. 2003. Variability of aerosol optical properties derived from in situ aircraft measurements during ACE-Asia. Journal of Geophysical Research 108, 8647. doi:10.1029/2002JD003247.

Anderson, T.L., Masonis, S.J., Covert, D.S., Charlson, R.J., Rood, M.J., 2000. In situ measurement of the aerosol extinction-to-backscatter ratio at a polluted continental site. Journal of Geophysical Research 105, 26907–26916.

Ansmann, A., Engelmann, R., Althausen, D., Wandinger, U., Hu, M., Zhang, Y., He, Q., Jul. 2005. High aerosol load over the Pearl River Delta, China, observed with Raman lidar and sun photometer. Geophysical Research Letters 32, 13815. doi:10.1029/2005GL023094.

Ansmann, A., Wandinger, U., Riebesell, M., Weitkamp, C., Michaelis, W., 1992. Independent measurement of extinction and backscatter profiles in cirrus clouds by using a combined Raman elastic-backscatter lidar. Applied Optics 31, 7113–7131.

Charlson, R.J., Schwartz, S.E., Hales, J.M., Cess, R.D., Coakley Jr., J.A., Hansen, J.E., Hofmann, D.J., Jan. 1992. Climate forcing by anthropogenic aerosols. Science 255, 423–430.

Chazette, P., Mar. 2003. The monsoon aerosol extinction properties at Goa during INDOEX as measured with lidar. Journal of Geophysical Research 108, 4187. doi:10.1029/2002JD002074.

Chen, W.N., Chang, S.Y., Chou, C.C.K., Chen, Y.W., Chen, J.P., 2007a. Study of relationship between water-soluble Ca^{2+} and lidar depolarization ratio for spring aerosol in the boundary layer. Atmospheric Environment 41, 1440–1455.

Chen, W.N., Tsai, F.J., Chou, C.C.K., Chang, S.Y., Chen, Y.W., Chen, J.P., 2007b. Optical properties of Asian dusts in the free atmosphere measured by Raman lidar at Taipei, Taiwan. Atmospheric Environment 41, 7698–7714.

Chen, W.-N., Lin, P.H., Chen, T.K., Chou, C.C.K., Chen, J.P., 2006. Diurnal cycle of mixing height measured by lidar. In: Nagasawa, C., Sugimoto, N. (Eds.), 23rd International Laser Radar Conference (ILRC 2006).

Cooper, D.W., Davis, J.W., Byers, R.L., 1974. Measurements of depolarization by dry and humidified salt aerosols using a lidar analogue. Aerosol Science 5, 117–123.

Draxler, R.R., Rolph, G.D., 2003. HYSPLIT (Hybrid Single-particle Lagrangian Integrated Trajectory) Model Access via NOAA ARL Ready Website. NOAA Air Resources Laboratory, Silver Spring, MD. <http://www.arl.noaa.gov/ready/hysplit4.html>.

Fernald, F.G., Mar. 1984. Analysis of atmospheric lidar observations: some comments. Applied Optics 23, 652–653.

Ferrare, R.A., Turner, D.D., Brasseur, L.H., Feltz, W.F., Dubovik, O., Tooman, T.P., Sep. 2001. Raman lidar measurements of the aerosol extinction-to-backscatter ratio over the Southern Great Plains. Journal of Geophysical Research 106, 20333–20348.

Franke, K., Ansmann, A., Müller, D., Althausen, D., Wagner, F., Scheele, R., 2001. One-year observations of particle lidar ratio over the tropical Indian Ocean with Raman lidar. Geophysical Research Letters 28, 4559–4562.

Hopkinson, L., Stern, R., 2002. One country, two systems, one smog cross-boundary air pollution policy challenges for Hong Kong and Guangdong. China Environment Series 6, 19–36.

Iwasaka, Y., Shibata, T., Nagatani, T., Shi, G.-Y., Kim, Y.S., Matsuki, A., Trochkine, D., Zhang, D., Yamada, M., Nagatani, M., Nakata, H., Shen, Z., Li, G., Chen, B., Kawahira, K., 2003. Large depolarization ratio of free tropospheric aerosols over the Taklamakan Desert revealed by lidar measurements: possible diffusion and transport of dust particles. Journal of Geophysical Research 108. doi:10.1029/2002JD003267.

Klett, J.D., Jan. 1981. Stable analytical inversion solution for processing lidar returns. Applied Optics 20, 211–220.

Klett, J.D., 1985. Lidar inversion with variable backscatter/extinction ratios. Applied Optics 24, 1638–1643.

Lin, C., Liu, S., Chou, C., Huang, S., Liu, C., Kuo, C., Young, C., 2005. Long-range transport of aerosols and their impact on the air quality of Taiwan. Atmospheric Environment 39, 6066–6076.

Lin, C.-Y., Liu, S.C., Chou, C.C.-K., Liu, T.H., Lee, C.-T., Yuan, C.-S., Shiu, C.-J., Young, C.-Y., 2004. Long-range transport of Asian dust and air pollutants to Taiwan. Terrestrial, Atmospheric and Oceanic Sciences 15, 759–784.

Lin, C.Y., Wang, Z., Chen, W.N., Chang, S.Y., Chou, C.C.K., Sugimoto, N., Zhao, X., 2007. Long-range transport of Asian dust and air pollutants to Taiwan: observed evidence and model simulation. Atmospheric Chemistry and Physics 7, 423–434.

Liu, S., Shiu, C., 2001. Asian dust storms and their impact on the air quality of Taiwan. Aerosol and Air Quality Research 1, 1–8.

Liu, Z., Sugimoto, N., Murayama, T., 2002. Extinction-to-backscatter ratio of Asian dust observed with high-spectral-resolution lidar and Raman lidar. Applied Optics 41, 2760–2767.

Ma, Y., Weber, R.J., Lee, Y.-N., Orsini, D.A., Maxwell-Meier, K., Thornton, D.C., Bandy, A.R., Clarke, A.D., Blake, D.R., Sachse, G.W., Fuelberg, H.E., Kiley, C.M., Woo, J.-H., Streets, D.G., Carmichael, G.R., Nov. 2003. Characteristics and influence of biosmoke on the fine-particle ionic composition measured in Asian outflow during the Transport and Chemical Evolution Over the Pacific (TRACE-P) experiment. Journal of Geophysical Research 108, 8816. doi:10.1029/2002JD003128.

Müller, D., Ansmann, A., Mattis, I., Tesche, M., Wandinger, U., Althausen, D., Pisani, G., Aug, 2007. Aerosol-type-dependent lidar ratios observed with Raman lidar. Journal of Geophysical Research 112, 16202. doi:10.1029/2006JD008292.

Murayama, T., Okamoto, H., Kaneyasu, N., Kamataki, H., Miura, K., 1999. Application of lidar depolarization measurement in the atmospheric boundary layer: effects of dust and sea-salt particles. Journal of Geophysical Research 104, 31781–31792.

Noh, Y., Kim, Y., Müller, D., 2008. Seasonal characteristics of lidar ratios measured with a Raman lidar at Gwangju, Korea in spring and autumn. Atmospheric Environment 42, 2208–2224.

Rolph, G.D., 2003. Real-time Environmental Applications and Display System (Ready) Website. NOAA Air Resources Laboratory, Silver Spring, MD. <http://www.arl.noaa.gov/ready/hysplit4.html>.

Sakai, T., Shibata, T., Iwasaka, Y., Nagai, T., Nakazato, M., Matsumura, T., Ichiki, A., Kim, Y.-S., Tamura, K., Troshkin, D., Hamdi, S., 2002. Case study of Raman lidar measurements of Asian dust events in 2000 and 2001 at Nagoya and Tsukuba, Japan. Atmospheric Environment 36, 5479–5489.

Sassen, K., 1991. The polarization lidar technique for cloud research: a review and current assessment. Bulletin of the American Meteorological Society 72, 1848–1866.

Sassen, K., 2002. Indirect climate forcing over the Western US from Asian dust storms. Geophysical Research Letters 29, 103–111.

Sassen, K., Zhao, H., Yu, B.-K., 1989. Backscatter laser depolarization studies of simulated stratospheric aerosols – crystallized sulfuric acid droplets. Applied Optics 28, 3024–3029.

Schuster, G.L., Dubovik, O., Holben, B.N., Apr. 2006. Angstrom exponent and bimodal aerosol size distributions. Journal of Geophysical Research 111, 7207. doi:10.1029/2005JD006328.

Seinfeld, J.H., Pandis, S.N., 1998. Atmospheric Chemistry and Physics: from Air Pollution to Climate Change. Wiley, New York, NY.

Shiu, C.-J., Chen, Y.-W., Chen, J.-P., Liu, S.C., Lin, P.-H., Lin, H.-J., Chen, W.-N., Chang, S.-Y., Hazra, A., Chou, C.C.K., Lung, S.-C., Hsu, S.-C., 2006. Correlation between aerosol optical depth derived from CIMEL sunphotometer and surface particulate concentration in Northern and Southern Taiwan. In: Society of Photo-Optical Instrumentation Engineers (SPIE) Conference Series, vol. 6299, p. 62990T. doi:10.1117/12.677997.

Streets, D.G., Yarber, K.F., Woo, J.-H., Carmichael, G.R., Oct. 2003. Biomass burning in Asia: annual and seasonal estimates and atmospheric emissions. Global Biogeochemical Cycles 17, 1099. doi:10.1029/2003GB002040.

Sugimoto, N., Matsui, I., Shimizu, A., Uno, I., Asai, K., Endoh, T., Nakajima, T., 2002. Observation of dust and anthropogenic aerosol plumes in the Northwest Pacific with a two-wavelength polarization lidar on board the research vessel Mirai. Geophysical Research Letters 29. doi:10.1029/2002GL015112.

Takamura, T., Sasano, Y., Hayasaka, T., Oct. 1994. Tropospheric aerosol optical properties derived from lidar, sun photometer, and optical particle counter measurements. Applied Optics 33, 7132–7140.

Twomey, S., 1991. Aerosols, clouds and radiation. Atmospheric Environment 25, 2435–2442.

van de Hulst, H.C., 1957. Light Scattering by Small Particles. John Wiley and Sons, New York.

Wandinger, U., Ansmann, A., 2002. Experimental determination of the lidar overlap profile with Raman lidar. Applied Optics 41, 511–514.

Wang, J., Xia, X., Wang, P., Christopher, S.A., 2004. Diurnal variability of dust aerosol optical thickness and Angstrom exponent over dust source regions in China. Geophysical Research Letters 31. doi:10.1029/2004GL019580.

Wang, S., Lin, N., Chou, M., Woo, J., 2007. Estimate of radiative forcing of Asian biomass-burning aerosols during the period of TRACE-P. Journal of Geophysical Research 112 (D10). doi:10.1029/2006JD007564.

Weber, A., Porto, S.P.S., Cheesman, L.E., Barrett, J.J., 1967. High-resolution Raman spectroscopy of gases with cw-laser excitation. Journal of the Optical Society of America 57, 19–28.

Welton, E., Voss, K., Quinn, P., Flatau, P., Markowicz, K., Campbell, J., Spinhirne, J., Gordon, H., Johnson, J., 2002. Measurements of aerosol vertical profiles and optical properties during INDOEX 1999 using micropulse lidars. Journal of Geophysical Research 107. doi:10.1029/2000JD000038.

Young, A.T., 1980. Revised depolarization corrections for atmospheric extinction. Applied Optics 19, 3427–3428.